

Discovery of the Zintl-phosphide BaCd_2P_2 as a long carrier lifetime and stable solar absorber

Zhenkun Yuan,¹ Diana Dahliah,^{2,3} Muhammad Rubaiat Hasan,⁴ Gideon Kassa,¹ Andrew Pike,¹ Shaham Quadir,⁵ Romain Claes,² Cierra Chandler,⁶ Yihuang Xiong,¹ Victoria Kyveryga,^{4,7} Philip Yox,^{4,7} Gian-Marco Rignanese,² Ismaila Dabo,⁶ Andriy Zakutayev,⁵ David P. Fenning,⁸ Obadiah G. Reid,^{5,9} Sage Bauers,⁵ Jifeng Liu,¹ Kirill Kovnir,^{4,7} and Geoffroy Hautier^{1,*}

*Corresponding author. Email: geoffroy.hautier@dartmouth.edu

1 Thayer School of Engineering, Dartmouth College, Hanover, NH 03755, USA

2 Institute of Condensed Matter and Nanosciences, Université Catholique de Louvain, Chemin des Étoiles 8, B-1348, Louvain-la-Neuve, Belgium

3 Department of Physics, An-Najah National University, Nablus, Palestine

4 Department of Chemistry, Iowa State University, Ames, IA 50011, USA

5 National Renewable Energy Laboratory, Golden, CO 80401, USA

6 Department of Materials Science and Engineering, and Materials Research Institute, The Pennsylvania State University, University Park, PA 16802, USA

7 Ames National Laboratory, U.S. Department of Energy, Ames, IA 50011, USA

8 Department of Nanoengineering, UC San Diego, La Jolla, CA 92093, USA

9 University of Colorado Boulder, Boulder, CO 80309, USA

Abstract

Thin-film photovoltaics offers a path to significantly decarbonize our energy production. Unfortunately, current materials commercialized or under development as thin-film solar cell absorbers are far from optimal as they show either low power conversion efficiency or issues with earth-abundance and stability. Entirely new and disruptive materials platforms are rarely discovered as the search for new solar absorbers is traditionally slow and serendipitous. Here, we use first principles high-throughput screening to accelerate this process. We identify new solar absorbers among known inorganic compounds using considerations on band gap, carrier transport, optical absorption but also on intrinsic defects which can strongly limit the carrier lifetime and ultimately the solar cell efficiency. Screening about 40,000 materials, we discover the Zintl-phosphide BaCd_2P_2 as a potential high-efficiency solar absorber. Follow-up experimental work confirms the predicted promises of BaCd_2P_2 highlighting an optimal band gap for visible absorption, bright photoluminescence, and long carrier lifetime of up to 30 ns even for unoptimized powder samples. Importantly, BaCd_2P_2 does not contain any critical elements and is highly stable in air and water. Our work opens an avenue for a new family of stable, earth-abundant, high-performance Zintl-based solar absorbers. It also demonstrates how recent advances in first principles computation can accelerate the search of photovoltaic materials by combining high-throughput screening with experiment.

Introduction

Photovoltaics (PV) will play a central role in the ongoing energy transition towards a sustainable, low-carbon-emission society.¹⁻³ In that regard, thin-film solar cells have remarkable prospects, because their manufacturing can require smaller upfront capital investment, less energy input and produces fewer greenhouse gas emissions than today's dominant silicon-based technology. Thin-film technologies can also offer compatibility with flexible substrates and band-gap tuning opportunities leading to building-integrated power generation or tandem devices in combination with silicon PV. Among the different materials used as solar cell absorbers, CdTe and Cu(In,Ga)Se₂ (CIGS) have achieved high power conversion efficiency of over 22% and have been commercialized for almost two decades.^{4,5} Unfortunately, CdTe and CIGS rely on critical elements, such as tellurium and indium, raising concerns for multi-terawatt scale deployment.^{6,7} Over the last decade, earth-abundant thin-film materials such as Cu₂ZnSn(S,Se)₄ (CZTS) and, in particular, lead halide perovskites (e.g., MAPbI₃, where MA=CH₃NH₃⁺) have emerged. However, CZTS lags behind commercial thin-film technologies in efficiency, while halide perovskites suffer from long-term stability issues.⁸⁻¹⁴

Large-scale deployment of thin-film PV demands high-efficiency, stable, and low-cost solar absorbers that are yet to be discovered. For over half a century, only a limited number of materials have been explored for thin-film PV applications,¹⁵⁻¹⁹ as conventional materials discovery is an intrinsically slow process. Most of the materials research efforts in the thin-film PV field have been devoted to modifying known semiconductors (cation substitution in CZTS,²⁰⁻²³ mixed-cation/mixed-halide perovskites,²⁴⁻²⁶ ...) but the recent advent of halide perovskites demonstrates that an unexpected new family of PV materials can still be found and revolutionize the field. This motivates further “out-of-the-box” explorative work, especially towards more stable materials than the halide perovskites.

High-throughput (HT) computational screening can significantly accelerate materials discovery and is emerging in the PV field.²⁷⁻³⁷ While earlier HT searches for solar absorbers focused on bulk properties, such as band gap, effective mass, and optical absorption coefficient,²⁷⁻³⁵ more complex properties related to point defects have started to be integrated into the screening as well.^{36,37} Considering defect-assisted nonradiative carrier recombination is essential in the search for new high-performance solar absorbers. Indeed, designing and discovering materials with “defect tolerance” and long carrier lifetime has become an important target for the PV community.³⁸⁻⁴⁵ Yet, only a few HT studies have included defect properties in the screening process, and their focus so far is mainly on copper-based inorganic materials³⁶ and perovskite compounds.³⁷ Moreover, these computational predictions have not yet lead to experimental realization of a proposed solar absorber.

Here, we identify the BaCd₂P₂ as a long carrier lifetime and stable solar absorber using HT computational screening followed by bulk synthesis and experimental characterization. We

perform HT search to screen about 40,000 inorganic materials obtained from the Materials Project database,⁴⁶ most of which are registered in the Inorganic Crystal Structure Database (ICSD).⁴⁷ We find a handful of materials combining a suitable band gap, small effective masses, and promising defect properties which will not cause strong nonradiative carrier recombination. Among these promising candidates, we select the Zintl-phosphide BaCd_2P_2 and explicitly show that the computed nonradiative recombination rates in BaCd_2P_2 are better than or comparable to those in high-efficiency solar absorbers such as the halide perovskites. We experimentally synthesize and characterize BaCd_2P_2 , showing that this material is highly stable in air and water. Bright photoluminescence (PL) and time-resolved microwave conductivity (TRMC) measurements confirm the computed direct band gap of 1.45 eV and present a promising long carrier lifetime of up to 30 ns. All of these results indicate that BaCd_2P_2 is a promising high-performance solar cell absorber with the potential to open a new avenue in PV for an entire family of Zintl AM_2X_2 solar absorbers (where A and M are +2 ions and X is a pnictogen).

Results and Discussion

High-throughput computational screening for high-efficiency solar absorbers

Our starting point is the Materials Project electronic structure database. Without constraints on any specific chemistry, we obtain 39,659 materials with full data on crystal structure, electronic band structure, and effective masses. We adopt a tiered computational screening approach (very similar to our previous work³⁶) to search for solar cell absorbers among these materials (see Note S1 of the supplemental information). Including electronic and defect properties in HT screening requires combining calculations at different levels of theory from (semilocal) Density Functional Theory (DFT) to more accurate but computationally expensive Heyd-Scuseria-Ernzerhof (HSE) hybrid functional.⁴⁸ Our screening consists of considering first DFT band gaps and effective masses, followed by a refinement of the band gap using the HSE hybrid functional and then defect computations combining DFT and HSE. Finally, we perform full HSE defect calculations for 19 candidates, and predict their solar-cell efficiency using an extended detailed-balance (i.e., Shockley-Queisser) model which accounts for defect-assisted nonradiative carrier recombination.^{36,49,50} At this screening stage we examine only vacancies and cation-cation antisites, without considering interstitials and cation-anion antisites. For nonradiative recombination, we assume a constant carrier capture cross section for all defects. This effectively penalizes materials with low-formation-energy, deep defects. Previous work has shown that this model can discriminate between high-performance solar absorbers and materials that are unlikely to realize high efficiency because of their defect properties.^{36,49,50}

The 19 candidates together with 12 established solar absorbers are displayed in Figure 1 with their

theoretical power conversion efficiency and estimated material cost (see Note S1 for more details). Additional metrics beyond cost related to production and earth abundance can also be found in Figures S2. Given that stability issues are hampering the deployment of halide perovskite solar cells, we have taken into account stability in selecting candidate materials. Unfortunately, there is no easy-to-compute criterion for assessing stability in realistic conditions. We can estimate the thermodynamic stability (energy above hull) of a material versus competing phases from DFT, but this is a poor indicator of stability in air and with respect to moisture. In fact, much of non-oxides (e.g., phosphides) show thermodynamic instability in contact with oxygen. Kinetic effects and surface passivation are likely to be key factors for their stability but are currently poorly assessed by theory. To assess stability, we rely on qualitative estimates based on the solid-state-chemistry experience of the authors and by following the literature report on these materials including the work reporting their synthesis. For instance, for the many alkali and alkaline-earth metal pnictides (phosphides, antimonides, ...) in the list, we have used a simple empirical rule: the higher the alkali or alkaline-earth per formula unit, the less stable the material will be. For example, according to this rule, KZnP (33%) should be less stable than BaCd₂P₂ (20%). Our stability assessment is conveyed in Figure 1 through the color of the data point.

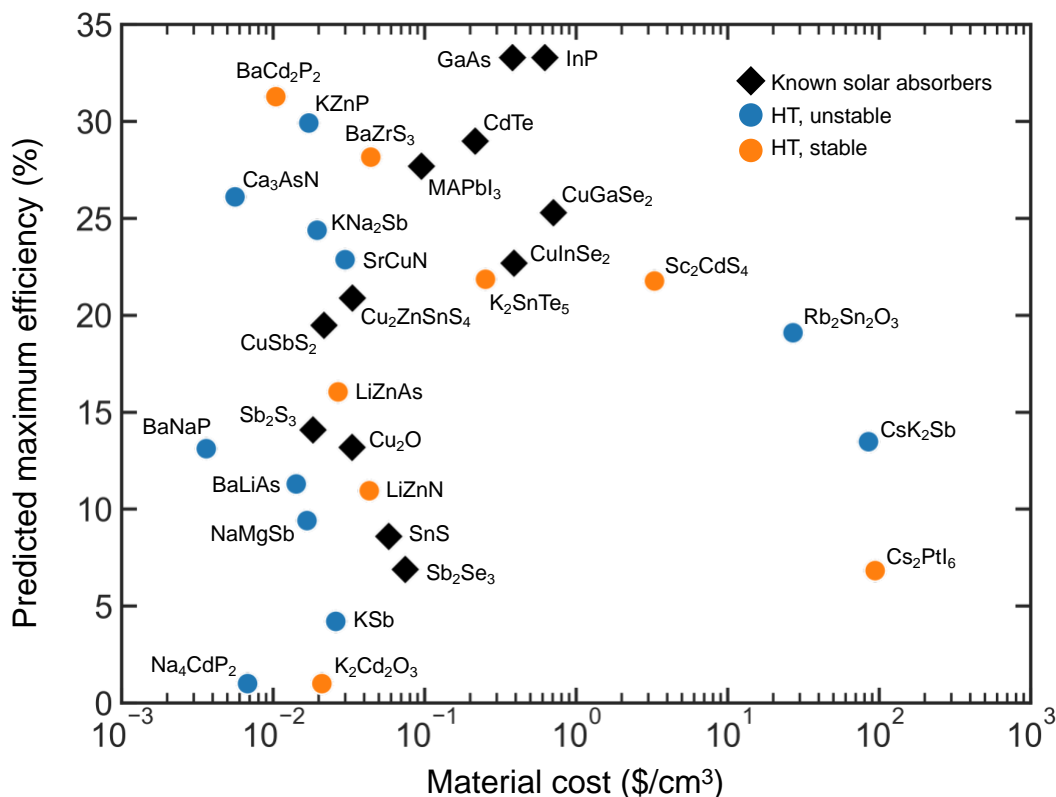


Figure 1 Theoretical power conversion efficiency versus material cost for 19 potential thin-film solar cell absorbers identified from high-throughput (HT) screening Black diamonds represent known thin-film solar absorbers for comparison purposes. Blue circles represent materials that are likely to be sensitive to air and moisture. Orange circles represent materials that are probably stable in air and moisture.

The most promising candidates when combining power conversion efficiency, materials cost, and stability are BaCd₂P₂ and BaZrS₃. The BaZrS₃ perovskite has recently been studied for thin-film PV applications.^{51,52} In contrast, BaCd₂P₂ is classified as a Zintl compound and has received little attention in the PV field since it was experimentally reported in the 1980s.^{53,54} While BaCd₂P₂ has recently been shown to possess a suitable band gap and small effective masses,^{32,55} our HT screening, which includes defect-assisted nonradiative recombination, makes it stand out from the vast number of materials with suitable band gaps. Other candidates such as the spinel ScCd₂S₄ or K₂SnTe₅ have cost and abundance issues. They are still of scientific interest and substitutional strategies could be considered to reduce or even eliminate the use of the critical elements (Sc and Te). Other interesting candidates such as KZnP, Na₂KSb, SrCuN, and Ca₃AsN are excluded due to stability concerns, confirmed by their experimental synthesis reports.⁵⁶⁻⁵⁹ Based on these considerations, we select BaCd₂P₂ as the most promising solar absorber candidate. In the following, we provide a more detailed study of the optoelectronic and defect properties of BaCd₂P₂.

BaCd₂P₂ computed bulk optoelectronic properties

BaCd₂P₂ crystallizes in the $P\bar{3}m1$ CaAl₂Si₂ Zintl-type structure⁶⁰ (Figure 2A). The crystal structure consists of alternating layers of tetrahedrally coordinated Cd and octahedrally coordinated Ba. This structure type has attracted substantial interest for thermoelectric applications, e.g., the antimonides Mg₃Sb₂ and CaMg₂Sb₂.⁶¹⁻⁶⁵ Figure 2B shows the BaCd₂P₂ band structure calculated with HSE. The direct band gap value of 1.45 eV is ideal for single-junction solar cells according to the detailed-balance model. There is a competing indirect gap which should not be detrimental to PV performance and, instead, has been suggested to be beneficial to carrier lifetime.^{66,67} The band structure exhibits dispersive valence and conduction bands. As a result, the effective masses are low for both electrons (0.11–0.74 m_0) and holes (0.44–0.63 m_0).⁶⁸ Further carrier mobility calculations including phonon scattering give a room-temperature mobility of 111–916 cm²/Vs for electrons and 123–242 cm²/Vs for holes depending on the crystallographic direction (Figure S3). The computed mobility is for a perfect single-crystal of BaCd₂P₂, and provides an upper bound for the mobilities in a polycrystalline film with impurities. While lower than in III-V semiconductors such as GaAs, the mobilities are comparable to those in many other solar absorbers such as CdTe,^{69,70} CZTS,⁷¹ and MAPI₃.⁷² Besides, as shown in Figure 2C, the computed optical absorption coefficient BaCd₂P₂ is over 10⁴ cm⁻¹ in the visible light range and is on par with those of known thin-film solar absorbers.

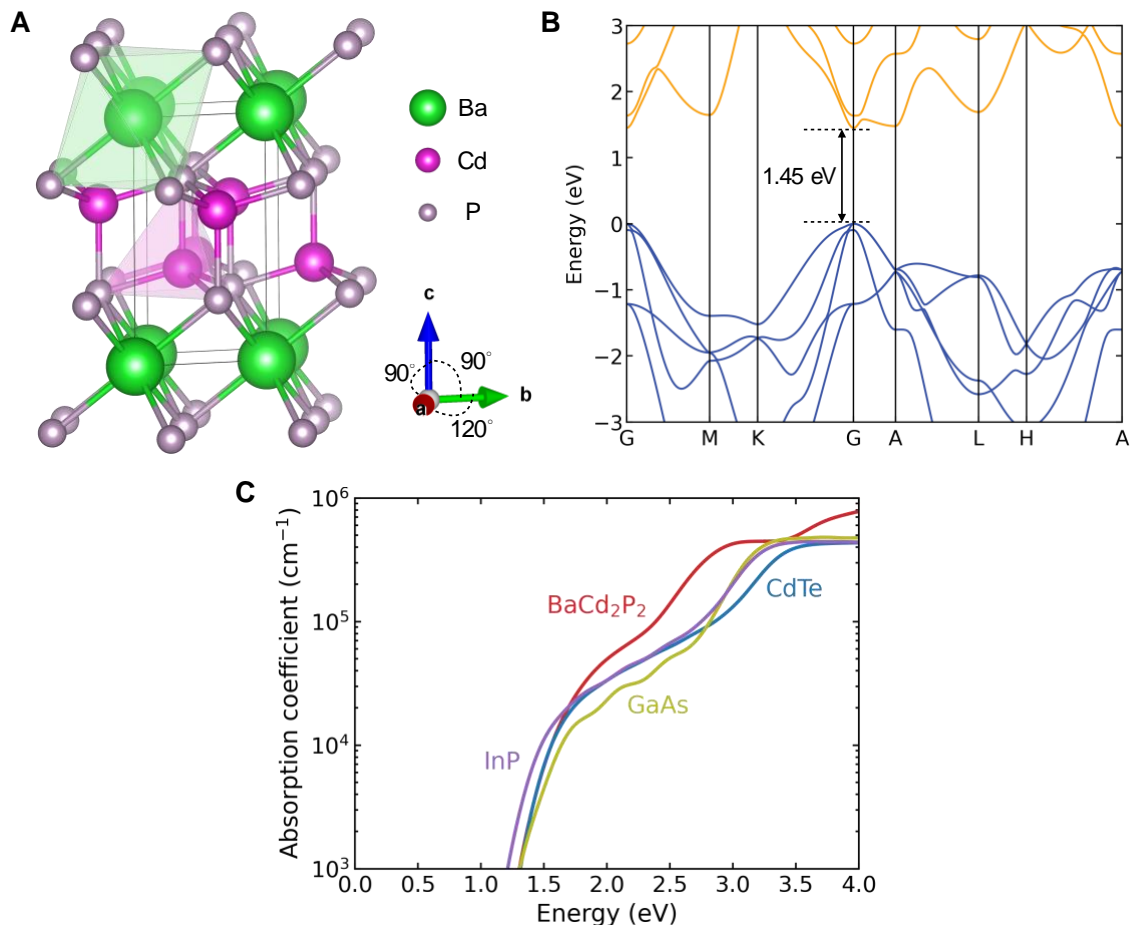


Figure 2 Crystal structure, electronic band structure, and optical absorption of BaCd₂P₂ (A) Crystal structure of BaCd₂P₂. Green octahedra and pink tetrahedra show the phosphorus coordination of Ba and Cd, respectively. (B) HSE electronic band structure of BaCd₂P₂ (C) Calculated optical absorption spectra of BaCd₂P₂. The absorption calculation is at the DFT-GGA-PBE level, with the band gap corrected using the HSE value. Also shown are the calculated optical absorption spectra for GaAs, CdTe, and InP at the same level of theory.

BaCd₂P₂ defect charge transition levels and dopability

Our HT screening has identified BaCd₂P₂ to be of interest not only for its band gap, carrier transport, and optical absorption but also for the absence of low-formation-energy, deep defects that can act as strong nonradiative recombination centers. In the initial screening, we considered only a limited types of intrinsic point defects. In the following, we provide a comprehensive first-principles study of intrinsic point defects in BaCd₂P₂. The electrical behavior of the defects is assessed based on their calculated formation energies and charge transition levels. The defect formation energy depends on the elemental chemical potentials which are related to synthesis conditions. The allowed chemical potentials of Ba, Cd, and P satisfy the stability condition of BaCd₂P₂, and are bound by the formation of different secondary phases in the Ba-Cd-P system (see Figure S4). Figures 3A and 3B plot the defect formation energies as a function of Fermi level

under P-poor and P-rich conditions (Figure S4), respectively. Formation energies at other chemical-potential conditions can be found in Figure S5.

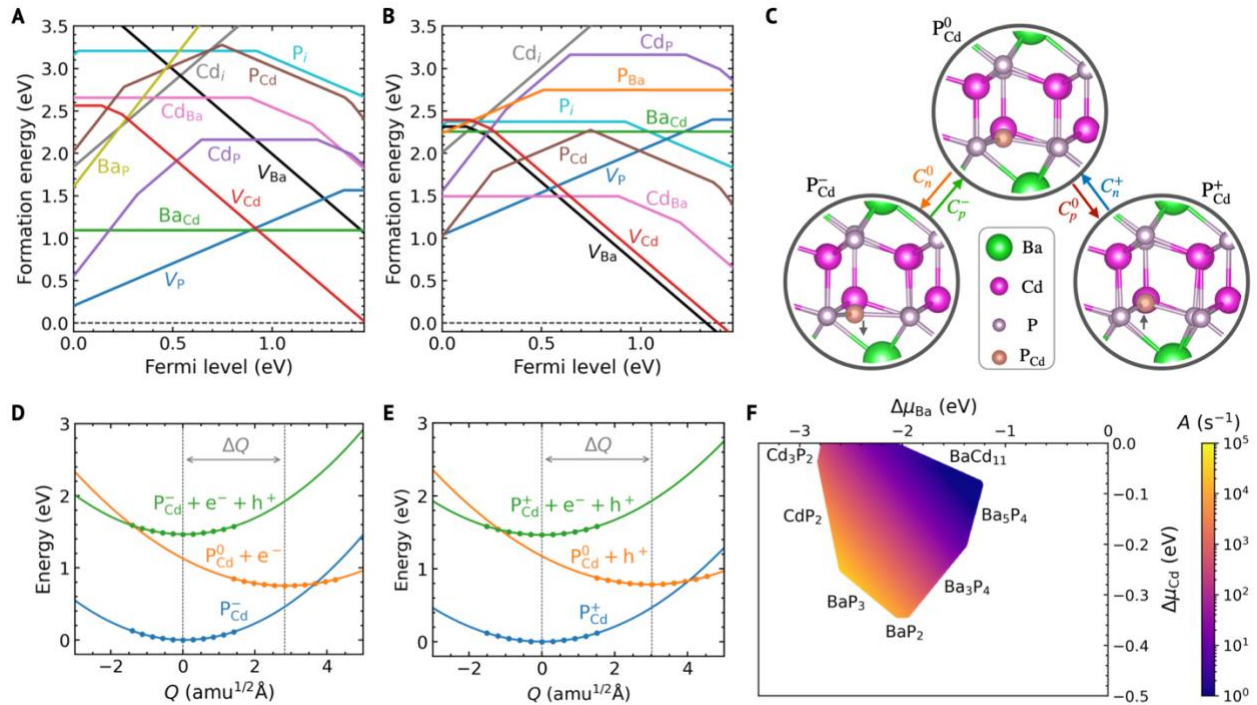


Figure 3 Formation energies of intrinsic point defects, carrier capture at the P_{Cd} antisite, and nonradiative carrier recombination in $BaCd_2P_2$ (A) and (B) HSE-calculated defect formation energies as a function of Fermi level under P-poor and P-rich conditions, respectively. (C) Local atomic structures of the P_{Cd} antisite in the 0, -1, and +1 charge states (see also Figure S8D). The gray arrows indicate the relaxation of the phosphorus antisite when charged. Transition between two adjacent charge states involves two carrier capture processes, as indicated by the colored arrows and the corresponding capture coefficients; for the capture coefficients, the superscript denotes the initial charge state and the subscript denotes the carrier type (n , electron; p , hole). (D) and (E) Configuration coordinate diagrams describing the P_{Cd} (0/-) and (0/+) charge-state transitions (see also Figures S8A–S8B), respectively. (F) Nonradiative recombination rates (denoted as A , in unit of s^{-1}) in intrinsic $BaCd_2P_2$ as a function of elemental chemical potentials in the $(\Delta\mu_{Ba}, \Delta\mu_{Cd})$ plane. The A rates are given by $A = C_{tot} \times N_d$. Here, only the dominant nonradiative center P_{Cd} is considered. The defect density (N_d) of P_{Cd} is computed at 1000 K, while the total capture coefficient (C_{tot}) of P_{Cd} is determined at 300 K.

Figures 3A and 3B show that vacancies are the dominant defect species in $BaCd_2P_2$: V_{Ba} and V_{Cd} are the dominant acceptors; V_P is the dominant donor. When ionized, the vacancies can have low formation energies for Fermi-level positions close to the band edges. Fortunately, they are all shallow defects, and can therefore be ruled out as nonradiative recombination centers. Early on in the study of lead halide perovskites, it was hypothesized that the long carrier lifetime and “defect tolerance” of $MAPI_3$ result from the shallow nature of vacancy defects.^{39,42,73-75} While for $MAPI_3$ this picture has been challenged by recent studies,⁷⁶⁻⁷⁸ $BaCd_2P_2$ clearly shows shallow vacancies for both cations and anions. The formation of shallow vacancies has been linked to the electronic structure of the material and, more specifically, to the presence of an antibonding upper valence band and a bonding lower conduction band.^{38,42,79} Indeed, for $BaCd_2P_2$, most of the upper valence bands consist of antibonding states between Cd $4d$ and P $3p$, and the lower conduction bands show

an overall bonding character which is a mix of bonding interactions between Cd $4p$, Ba $4d$, and Ba $6s$ (though antibonding interactions between Cd $4d$ and P $3p$ are also observed) (Figure S6). We note that the bonding character of the lower conduction bands of BaCd_2P_2 arising from two types of cations is not common, suggesting that chemical bonding can be more complex in materials and that interaction beyond cation-anion orbital overlap can determine the electronic structure.

Some of the antisite defects in BaCd_2P_2 can also be low in formation energy, notably for Ba_{Cd} and Cd_{Ba} . Given the large difference in ionic radii between Cd^{2+} and Ba^{2+} (1.09 Å vs 1.49 Å), one would expect that it should be energetically much less favorable to form Ba_{Cd} than Cd_{Ba} . However, our previous analysis has shown no clear correlation between ionic size difference and antisite formation energy.³⁶ What our previous study found, however, is that elements with similar preferred oxidation states tend not to form antisites with deep levels. This is the case here for Ba occupying the site of smaller Cd but surprisingly not for Cd replacing the larger Ba. The Ba_{Cd} introduces no defect level in the band gap of BaCd_2P_2 , as expected. By contrast, Cd_{Ba} is a deep double acceptor. This may be understood from the larger antisite space of Cd_{Ba} , in which not only Cd^{2+} but also Cd^+ and Cd^0 with bigger ionic size can form. Both the P_{Cd} and Cd_{P} antisites are amphoteric with deep levels. The amphoteric behavior of these two antisites may be linked to the oxidation behavior of P which can act both as a cation and anion and have oxidation states spanning from +5 to -3 . The interstitials have overall high formation energies and should not be a concern for nonradiative carrier recombination. Based on these results, we will later assess quantitatively the effectiveness of Cd_{Ba} , P_{Cd} , and Cd_{P} as nonradiative recombination centers. We note that cation-anion antisites have also been found to form deep defects in other phosphide solar absorbers such as InP^{80} and Zn_3P_2 .⁸¹

The defect formation energies plotted in Figures 3A–3B and S5 provide important insights into doping in BaCd_2P_2 . Irrespective of the elemental chemical potentials, BaCd_2P_2 clearly will not be highly doped either p -type or n -type by the intrinsic point defects. The equilibrium Fermi-level position, which can be estimated to be near the crossing point between the formation-energy curves for the dominant acceptor and donor species (such as V_{Cd} and V_{P} in Figure 3A), never gets close to the band edges, implying very low free carrier concentration. Extrinsic acceptor doping could potentially make BaCd_2P_2 p -type doped, especially under the P-rich condition where the V_{P} donor and other donor defects have overall high formation energies meaning weak compensation (Figure 3B). In contrast, n -type doping in BaCd_2P_2 is likely to be challenging, due to strong compensation from V_{Ba} and V_{Cd} , whose formation energies can drop to nearly or even below zero for Fermi-level positions close to the conduction-band minimum (CBM). This doping asymmetry agrees with the relatively high absolute energy of the valence-band edge of BaCd_2P_2 (see Table S1).^{82,83} We conclude that BaCd_2P_2 is a natively semi-insulating material with high potential of realizing good p -type doping. It could be used as an intrinsic layer in a p - i - n junction or as a p -type layer in a p - n junction.

Deep defects and nonradiative recombination in BaCd₂P₂

Strong nonradiative carrier recombination requires deep defects with a high enough concentration but also large carrier capture coefficients.^{84–86} From the above (Figures 3A–3B), the deep defects with low formation energies are Cd_{Ba}, P_{Cd}, and Cd_P. The capture coefficients can be calculated from first principles considering nonradiative transition between the deep defect level and an electron at the CBM or a hole at the valence-band maximum (VBM) via multiphonon emission (details in Note S2). Here, we calculate capture coefficients for Cd_{Ba}, P_{Cd}, and Cd_P, and determine nonradiative carrier recombination rates in BaCd₂P₂. We assume an intrinsic BaCd₂P₂ absorber layer in a *p-i-n* device.

The Cd_{Ba} gives rise to a deep (0/−) level at 0.89 eV above the valence band (Figures 3A–3B). However, the configuration coordinate diagram for Cd_{Ba} (0/−) transition indicates that the electron capture barrier by Cd_{Ba}⁰ and the hole capture barrier by Cd_{Ba}[−] are both large (Figure S7A). Therefore, without explicitly computing the capture coefficients, Cd_{Ba} should not be a strong recombination center. The P_{Cd} has a (+/−) transition level near the mid gap. The direct transition between −1 and +1 states will not be efficient, due to the low probability for a defect capturing two electrons (or two holes) at once.⁸⁷ The recombination process of P_{Cd} can be treated by including the unstable neutral charge state ($q = 0$) and through two steps involving the (0/−) and (0/+) transition levels, as previously done for the iodine interstitial (I_i) in MAPI₃.⁸⁸ This amounts to four capture processes and coefficients in total: C_n^0 and C_n^+ for electron (n) capture and C_p^0 and C_p^- for hole (p) capture, as shown in Figure 3C. The P_{Cd} (0/−) and (0/+) levels are also very deep and locate 0.71 and 0.78 eV above the VBM, respectively (Figures S8A–S8B). Figures 3D and 3E show the configuration coordinate diagrams for the P_{Cd} (0/−) and (0/+) transitions, respectively. All four capture processes have small energy barriers, which qualitatively indicates that the capture processes by P_{Cd} can be easy. Quantitatively, for P_{Cd}, our calculations including electron-phonon coupling yield a total capture coefficient (C_{tot}) of 2.77×10^{-7} cm³/s at 300 K (see Figure S8C), which is significant but comparable to that of the most active recombination center (I_i) in MAPI₃.^{86,88} The local atomic structures of P_{Cd}⁰, P_{Cd}[−], and P_{Cd}⁺ plotted in Figure 3C highlights large displacements of the phosphorus antisite as a result of the charge transitions: the electron (hole) capture by P_{Cd}⁰ leads to a downward (upward) displacement of the phosphorus antisite, and P_{Cd}[−] (P_{Cd}⁺) shows a trigonal planar (trigonal pyramidal) P₄ configuration with three equidistant P-P bonds. The Cd_P antisite gives rise to a deep (0/2+) level as well. Compared to P_{Cd}, Cd_P presents a negligibly small C_{tot} at 300 K, mainly due to large hole capture barriers (Figures S7B–S7C; Table S3).

The above results indicate that P_{Cd} is the most efficient nonradiative recombination center in BaCd₂P₂, followed by Cd_P, and that Cd_{Ba} is inactive. In the following, we determine the nonradiative recombination rates in intrinsic BaCd₂P₂ at 300 K (see Note S2). The nonradiative recombination rate (denoted as A) is given by $A = C_{\text{tot}} \times N_{\text{d}}$, where C_{tot} and N_{d} are the total

capture coefficient and concentration of a recombination center, respectively. Figure 3F plots the nonradiative recombination rate A in intrinsic BaCd_2P_2 as a function of the elemental chemical potentials which control defect formation energy and concentration. The recombination rate is larger under P-rich conditions which favor the formation of P_{Cd} . Remarkably, the recombination rate is at most $\sim 10^5 \text{ s}^{-1}$, which are orders of magnitude smaller than that of MAPbI_3 ($\sim 10^7 \text{ s}^{-1}$, computed at a similar level of theory).^{86,88} This is because the P_{Cd} concentration is rather low (on the order of 10^{11} cm^{-3} or less) in intrinsic BaCd_2P_2 . Indeed, the lowest formation energy of P_{Cd} even under the extreme P-rich condition is higher than 1.0 eV (see Figure 3A), which is still larger than the highest formation energy of the I_i in MAPbI_3 under iodine-rich condition.⁸⁸ We also emphasize that the C_{tot} of P_{Cd} is comparable to that of I_i in MAPbI_3 . Using the calculated A rates, the nonradiative lifetime ($= 1/A$) in intrinsic BaCd_2P_2 is on the order of at least $10 \mu\text{s}$, indicating the potential for remarkably long bulk carrier lifetime.

If BaCd_2P_2 is used as a p -type absorber layer in a p - n junction, the carrier capture behavior changes. In p -type BaCd_2P_2 , the electron capture coefficients will dominate the total capture coefficient (Note S2; Table S3). As a consequence, not only P_{Cd} but also Cd_{P} will act as nonradiative centers. In addition, the P_{Cd} and Cd_{P} concentrations will be orders of magnitude higher when the Fermi level gets closer to the valence band (Figures 3A–3B). Assuming that the Fermi level is 0.2 eV above the VBM, the nonradiative recombination rates are $\sim 10^6$ – 10^8 s^{-1} (Figure S9). Such values are still on par with those in standard inorganic p -type solar absorbers CdTe ,^{89,90} CIGS ,⁹¹ and CZTS ,^{92,93} where the computed A rates of $\sim 10^7 \text{ s}^{-1}$ have been typically reported.

Synthesis and stability of BaCd_2P_2

All of our computational results (band gap, optical absorption, carrier mobilities, intrinsic point defects, and nonradiative carrier recombination at deep defects) highlight BaCd_2P_2 as a potentially high-performance inorganic solar absorber made of low-cost elements. BaCd_2P_2 was reported experimentally, but no experimental characterization of the optoelectronic properties of this material had been made.^{53,54} We have synthesized BaCd_2P_2 powder samples by solid-state reaction of the elemental Ba, Cd, and P in stoichiometric ratio in sealed silica ampoules. Details about the synthesis and characterization of the crystal structure and phase stability are provided in Notes S3–S6 of the supplemental information. Figure 4A plots the powder X-ray diffraction (PXRD) pattern of the BaCd_2P_2 sample, which shows no coexistence of secondary phases and confirms the previously reported crystal structure. The crystal lattice parameters obtained from PXRD Rietveld refinement agree well with previous measurements and our calculations (see Table S4).

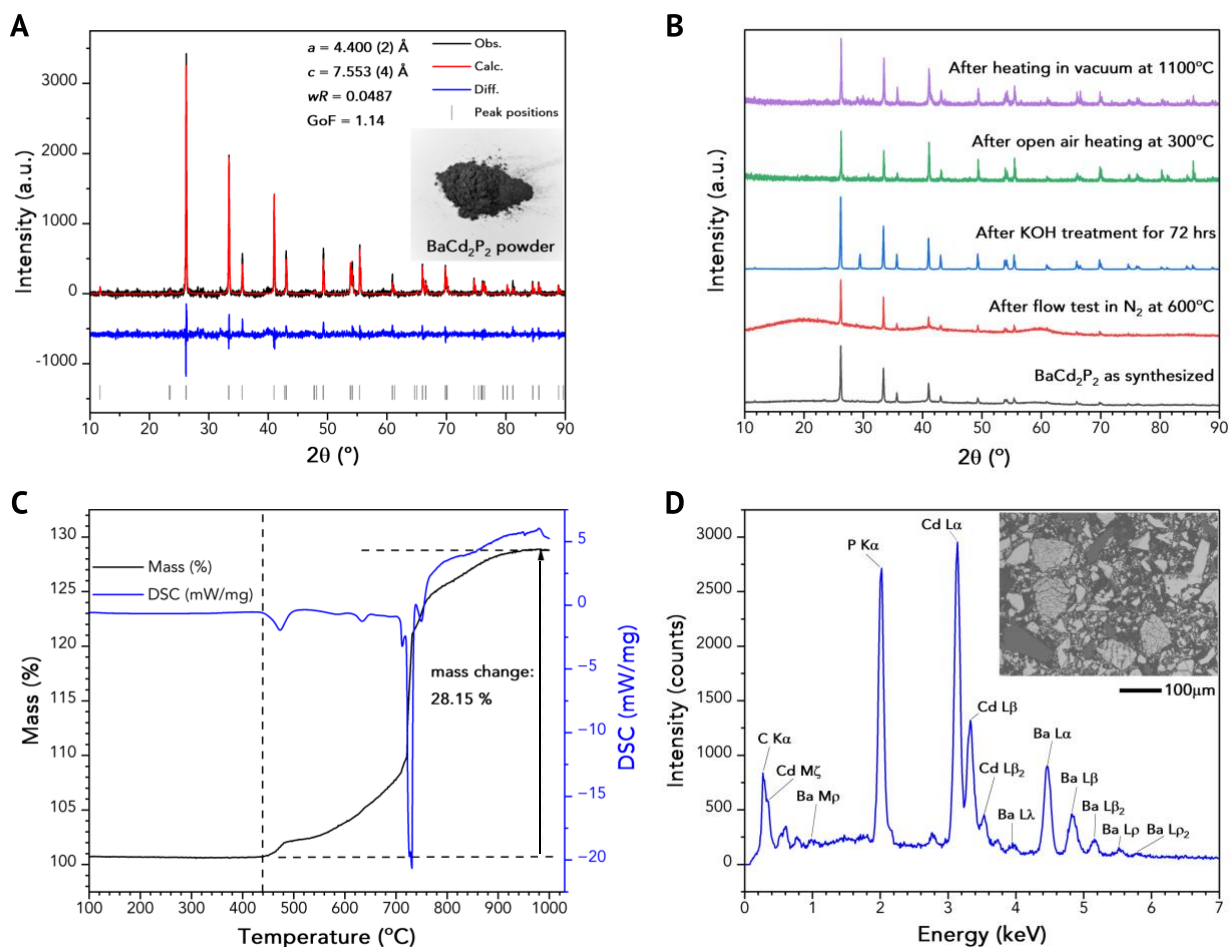


Figure 4 Characterization of crystal structure and phase stability of BaCd₂P₂ polycrystalline sample (A) PXRD pattern with Rietveld refinement for as-synthesized BaCd₂P₂ sample. (B) PXRD patterns of the BaCd₂P₂ samples after stability tests under various conditions. (C) TGA and DSC analysis of the thermal behavior of BaCd₂P₂ in air atmosphere. (D) Representative EDX spectra of BaCd₂P₂ with SEM image.

As highlighted by halide perovskites whose applications are limited by their stability,¹⁰⁻¹² air- and moisture-sensitivity has become an important concern for the technological deployment of new solar cell absorbers. We find that BaCd₂P₂ is highly stable in ambient air (for more than 6 months at room temperature), and that immersing a sample in water for 12 hours causes no appreciable changes in the PXRD pattern. Besides, BaCd₂P₂ is also found to be resistant to 2.5M KOH solution for at least 72 hours, probably due to passivation of surface with hydroxide as indicated by the appearance of a small PXRD peak at 29° corresponding to Cd(OH)₂ (Figure 4B). Only strong acids such as HCl, concentrated HNO₃, and *aqua regia* can dissolve BaCd₂P₂. PXRD pattern of BaCd₂P₂ after heating in open air at 300 °C shows no significant change in crystal structure (Figure 4B). PXRD taken after a flow test in N₂ gas reveals the sample to be stable even at 600 °C. In vacuum, annealing at temperatures up to 1100 °C results in no changes attested by the alike PXRD patterns. During thermogravimetric analysis (TGA) and differential scanning calorimetry (DSC) in ambient atmosphere, BaCd₂P₂ does not show any appreciable change until 425 °C after which the material starts to oxidize (Figures 4C and S10–S11). Morphology and overall stoichiometry of the

synthesized BaCd_2P_2 are examined using scanning electron microscopy (SEM) and electron-dispersive X-ray spectroscopy (EDS) (Figures 4D and S12–S13). The EDS analysis reveals a nearly stoichiometric BaCd_2P_2 sample and importantly no impurity phases in the sample. Overall, all these results demonstrate a very stable BaCd_2P_2 material, for which oxidation is probably kinetically limited and which should not require complex encapsulation and cumbersome processing.

Photoluminescence (PL) and carrier lifetime in BaCd_2P_2 powder

We have performed optoelectronic characterization of the BaCd_2P_2 powder samples. PL spectra are collected using a micro-PL setup in air, which allows us to target individual grains and conduct a statistical analysis of the PL intensity (see details in Note S7). Figure 5A shows a pronounced PL peak at 1.46 eV (847 nm) at 298 K, in very good agreement with the HSE band gap (1.45 eV) as well as the step in the transmittance spectra of BaCd_2P_2 (shown in the same figure). This suggests that the PL peak at 847 nm is due to band-to-band radiative recombination. A weaker PL peak at 980 nm (1.27 eV) is also observed, probably due to a shallow defect level close to the band edge. Characterizing this second peak will be the focus of our future work. Notably, the intensity of the PL peaks only slightly decreases when the sample is heated up to 368 K, and is fully recovered upon cooling back to 298 K (Figure 5A). The robust and strong PL spectra confirms that BaCd_2P_2 is also highly stable in terms of its optoelectronic properties in the entire temperature range of 298–323 K for typical solar cell operation.⁹⁴

To assess the PL efficiency more quantitatively and benchmark it versus a well-studied solar cell material, we compare in Figure 5B the PL spectra of BaCd_2P_2 and GaAs powders under identical excitation conditions. The GaAs sample is obtained by pulverizing a piece of device-grade single-crystal prime GaAs (001) wafer into a fine powder. GaAs is chosen because it is a well-established high-efficiency solar material and has a similar band gap. The BaCd_2P_2 and GaAs powder samples have similar particle sizes (Figure S14), so we expect comparable degrees of surface recombination and multiple scattering optical losses in both samples. Remarkably, Figure 5B shows that the PL peak intensity of our unoptimized BaCd_2P_2 is already in the same order as that of high-purity prime GaAs (i.e., only ~3 times weaker). This is also clearly seen in Figure 5B inset which shows the statistical histograms for 100 random spots on each sample. The result is encouraging, since BaCd_2P_2 , as a new solar material, lacks the level of purity of the prime single-crystal GaAs wafer.

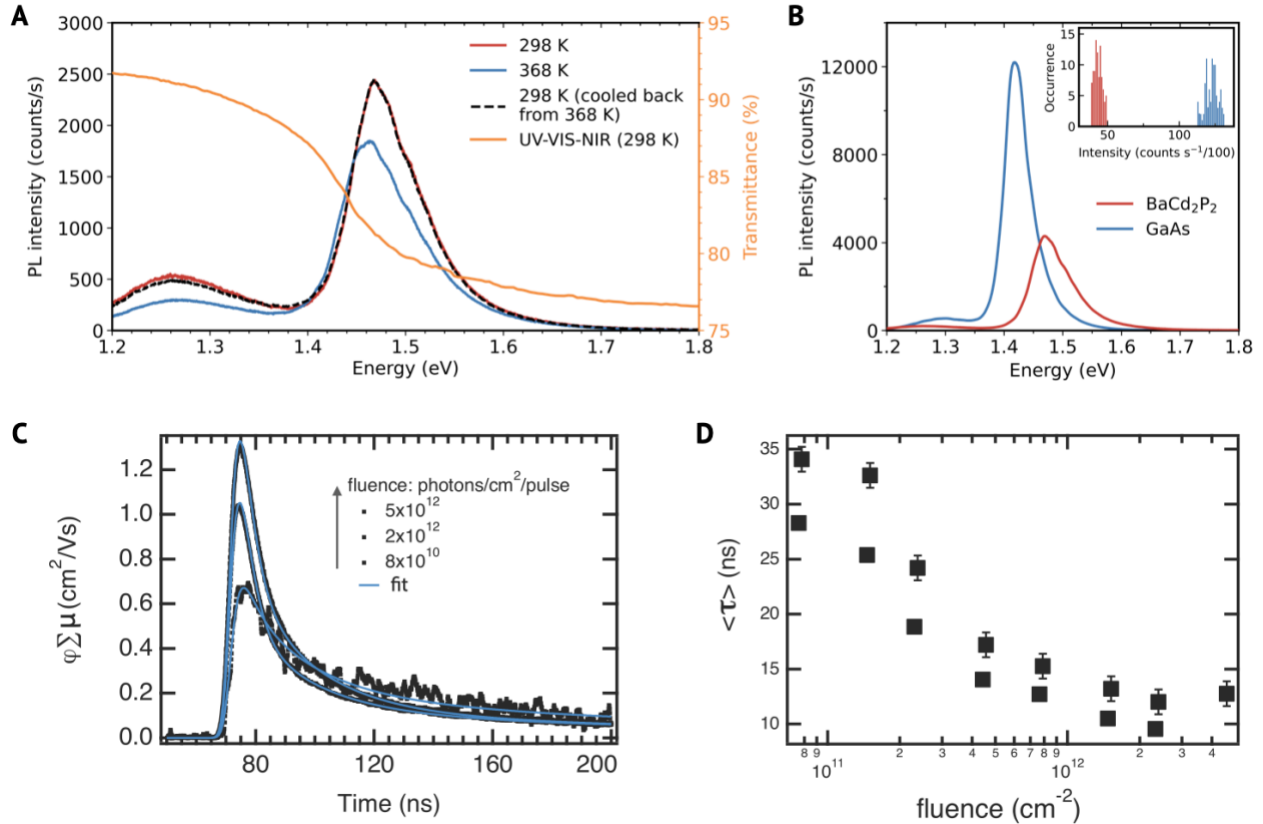


Figure 5 Photoluminescence (PL) and microwave conductivity measurements of BaCd_2P_2 polycrystalline samples (A) Comparison between PL spectra at 298 K, 368 K, and after cooling down the sample from 368 K back to 298 K. (B) Average micro-PL spectra of BaCd_2P_2 powder versus that of GaAs powder. The inset histograms count the occurrence of the PL intensity across the powders (C) Three representative photoconductivity transients (black) and tri-exponential fits (blue) as a function of laser fluence (600 nm, 7 ns FWHM), expressed as the product of carrier yield (φ) and mobility sum ($\Sigma\mu$). (D) Population-weighted average carrier lifetime $\langle \tau \rangle$ extracted from the tri-exponential fit to all transients collected for two sample replicates as a function of incident laser fluence.

For a more quantitative study of carrier transport and excited-state dynamics in BaCd_2P_2 , we have performed time-resolved and steady-state microwave conductivity (TRMC^{95,96} and SSMC⁹⁷) measurements on BaCd_2P_2 powder (see Note S8). Microwave conductivity measurements employ a microwave field to probe the conductive and dielectric properties of semiconductor materials without the need for electrical contacts, making it particularly suitable for characterizing powder samples of emerging materials before high-quality thin films are available. Here, we analyze the equilibrium (i.e., dark) properties of the BaCd_2P_2 powder (Figure S15A), its transient carrier dynamics (Figures 5C–5D and S15B), and its photoconductivity action spectrum (Figure S16). Figure 5C shows photoconductivity transients expressed as a product of charge carrier yield and mobility sum for three representative laser fluences (see also Figure S15B). The blue solid lines show a fit to the data employing three exponential decay components, from which the population-weighted average carrier lifetime is calculated. As seen in Figure 5D, the carrier lifetime is within 10–30 ns depending on fluence; lower fluences result in longer lifetimes. An up to 30 ns photoconductivity lifetime is promising for unoptimized BaCd_2P_2 powders, since the surface

recombination effects are likely at play. For comparison, such a carrier lifetime already exceeds those measured for CdTe (before 2014)⁹⁸ and CZTS (present) thin-films.⁹⁹ Even halide perovskites, which are well known for their long carrier lifetimes, started with lifetimes of a few to a few hundred ns measured on thin films.^{100,101} As discussed above, carrier lifetime is strongly correlated with the efficiency potential and prospect of a new solar cell absorber.¹⁰²

The yield-mobility product extracted from TRMC provides a weighted sum of the electron and hole mobilities,^{103,104} assuming that every absorbed photon creates an unbound electron-hole pair ($\varphi = 1$). Here, we calculate its value using the sum of the pre-exponential factors from the fits in Figure 5C so as to account for recombination that occurs within the instrument response function.¹⁰⁵ These values are also fluence-dependent. Interestingly, the yield-mobility product *increases* with fluence, from 1 cm²/Vs at the lowest fluence to 4 cm²/Vs at the highest fluence (see also Figure S15B). Similar behavior is observed in steady-state photo-modulation (Figure S16B), where photoconductivity rises superlinearly ($\Delta\sigma \propto F^{1.5}$) with light flux (F). Under most circumstances the steady-state photoconductivity is expected to be either linear (first-order recombination) or sublinear ($\Delta\sigma \propto F^{0.5}$ for bimolecular recombination). Both our observations suggest that the present mobility and lifetime results are limited by a significant population of trap sites: as the injection density increases and traps become filled, the average carrier mobility increases.¹⁰⁶ This observation could be associated with the high-surface-area of the powder under investigation (Figure 4D inset). The steady-state photoconductivity action spectra (Figure S16A) and the PL spectra (Figure 5A) are consistent with this surface trap hypothesis. The former exhibits a non-zero tail to the red of the evident absorption onset near 855 nm (i.e., 1.45 eV), and the latter shows a broad second emission peak in the same region.

Finally, we note that the powder measured by TRMC has a XRD coherence length of only ~100 nm (Note S8), which likely suggests that the microwave frequency-dependent mobilities reported above are severely limited by the scattering effects due to crystalline grain boundaries or extended structural defects. Indeed, using a confinement length of 100 nm and an observed 9.6-GHz mobility of 4 cm²/Vs we get an intrinsic mobility of ~100 cm²/Vs (Figure S17), in agreement with the computed mobilities. It is worth noting that in the early-stage development of halide perovskite solar cells, the carrier mobilities in MAPI₃ were also within the order of magnitude measured for BaCd₂P₂ but increased with improvements in film quality.¹⁰⁷

Conclusions

We have computationally screened about 40,000 materials searching for high-efficiency, stable, and low-cost thin-film solar cell absorbers. A handful of solar absorber candidates have emerged and among them BaCd₂P₂ stands out for its computed direct band gap (1.45 eV), high carrier

mobilities, large optical absorption coefficients, and most importantly favorable point-defects which will not lead to strong nonradiative carrier recombination. BaCd_2P_2 is also made of low-cost and non-critical elements. Carrier capture calculations show that P_{Cd} is the dominant nonradiative recombination center, but its high formation energy leads to a very long nonradiative lifetime, at least two orders of magnitude higher than that of MAPI_3 .

Our synthesized BaCd_2P_2 powder samples show an experimental band gap in good agreement with theory and exhibit bright PL on par with the luminescence of a high-purity GaAs wafer powder. TRMC measurements on unoptimized powder indicate a carrier lifetime of up to 30 ns, which surpasses early halide perovskites thin films and is on par with present-day established inorganic PV absorbers. This experimentally confirms the promises of BaCd_2P_2 as a new thin-film solar absorber. In addition to its exceptional optoelectronic and defect properties, BaCd_2P_2 shows extremely high stability in air and water. It is stable in air for more than 6 months at room temperature, and oxidation only starts for temperature above 400 °C. The high stability will benefit the future development of BaCd_2P_2 solar cells.

The attractive properties of BaCd_2P_2 as a thin-film absorber material motivate the future growth of high-quality thin films and fabrication of solar cells with either a *p-n* or *p-i-n* junction device architecture. We note that several other phosphides crystallize in the BaCd_2P_2 structure type including the less toxic Zn-based CaZn_2P_2 and SrZn_2P_2 . In view of the exceptional properties exhibited by BaCd_2P_2 , these zinc-based compounds are of interest for future studies. The large family of Zintl BaCd_2P_2 structure type materials can offer opportunities for tuning band gap and other properties through elemental substitutions.

Beyond BaCd_2P_2 , our work highlights how high-throughput computational screening including point-defect properties and follow-up experimental synthesis and characterizations can identify unexpected solar absorbers with exceptional intrinsic PV properties among tens of thousands of materials. It paves the way for more computation-driven materials discovery in the PV field.

Acknowledgments

This work was supported by the U.S. Department of Energy, Office of Science, Basic Energy Sciences, Division of Materials Science and Engineering, Physical Behavior of Materials program under award number DE-SC0023509 to Dartmouth and was authored in part by the National Renewable Energy Laboratory, operated by Alliance for Sustainable Energy, LLC, for the U.S. Department of Energy (DOE) under Contract No. DE-AC36-08GO28308. All computations, syntheses, and characterizations were supported by this award unless specifically stated otherwise. This research used resources of the National Energy Research Scientific Computing Center (NERSC), a DOE Office of Science User Facility supported by the Office of Science of the U.S.

Department of Energy under contract no. DE-AC02-05CH11231 using NERSC award BES-ERCAP0023830. A. P. acknowledges support from a Department of Education GAANN fellowship. Funding for microwave conductivity measurements and analysis on semiconductor powders provided by the Materials Chemistry Program, Materials Sciences and Engineering Division, Office of Basic Energy Sciences, U.S. Department of Energy under grant DE-SC0023316. PPMS instrument used for initial attempts of conductivity measurements was supported by Ames National Laboratory, U.S. Department of Energy, which operates under the Contract DE-AC02-07CH11358. The views expressed in the article do not necessarily represent the views of the DOE or the U.S. Government.

References

1. Haegel, N.M., Verlinden, P., Victoria, M., Altermatt, P., Atwater, H., Barnes, T., Breyer, C., Case, C., De Wolf, S., Deline, C., et al. (2023). Photovoltaics at multi-terawatt scale: Waiting is not an option. *Science* *380*, 39-42. doi:10.1126/science.adf6957.
2. van Sark, W. (2023). Photovoltaics performance monitoring is essential in a 100% renewables-based society. *Joule* *7*, 1388-1393. <https://doi.org/10.1016/j.joule.2023.06.012>.
3. Jäger-Waldau, A. (2023). Snapshot of Photovoltaics – May 2023. *EPJ Photovolt.* *14*, 23.
4. Green, M.A., Dunlop, E.D., Yoshita, M., Kopidakis, N., Bothe, K., Siefert, G., and Hao, X. (2023). Solar cell efficiency tables (version 62). *Progress in Photovoltaics: Research and Applications* *31*, 651-663. <https://doi.org/10.1002/pip.3726>.
5. Mallick, R., Li, X., Reich, C., Shan, X., Zhang, W., Nagle, T., Bok, L., Bicakci, E., Rosenblatt, N., Modi, D., et al. (2023). Arsenic-Doped CdSeTe Solar Cells Achieve World Record 22.3% Efficiency. *IEEE Journal of Photovoltaics* *13*, 510-515. 10.1109/JPHOTOV.2023.3282581.
6. Candelise, C., Winkler, M., and Gross, R. (2012). Implications for CdTe and CIGS technologies production costs of indium and tellurium scarcity. *Progress in Photovoltaics: Research and Applications* *20*, 816-831. <https://doi.org/10.1002/pip.2216>.
7. Zhang, Y., Kim, M., Wang, L., Verlinden, P., and Hallam, B. (2021). Design considerations for multi-terawatt scale manufacturing of existing and future photovoltaic technologies: challenges and opportunities related to silver, indium and bismuth consumption. *Energy & Environmental Science* *14*, 5587-5610. 10.1039/D1EE01814K.
8. Zhao, Y., Ma, F., Qu, Z., Yu, S., Shen, T., Deng, H.-X., Chu, X., Peng, X., Yuan, Y., Zhang, X., and You, J. (2022). Inactive (PbI₂)₂RbCl stabilizes perovskite films for efficient solar cells. *Science* *377*, 531-534. doi:10.1126/science.abp8873.
9. Park, J., Kim, J., Yun, H.-S., Paik, M.J., Noh, E., Mun, H.J., Kim, M.G., Shin, T.J., and Seok, S.I. (2023). Controlled growth of perovskite layers with volatile alkylammonium chlorides. *Nature* *616*, 724-730. 10.1038/s41586-023-05825-y.
10. Stoumpos, C.C., Malliakas, C.D., and Kanatzidis, M.G. (2013). Semiconducting Tin and Lead Iodide Perovskites with Organic Cations: Phase Transitions, High Mobilities, and Near-Infrared Photoluminescent Properties. *Inorganic Chemistry* *52*, 9019-9038. 10.1021/ic401215x.
11. Meng, L., You, J., and Yang, Y. (2018). Addressing the stability issue of perovskite solar cells for commercial applications. *Nature Communications* *9*, 5265. 10.1038/s41467-018-07255-1.
12. Conings, B., Drijkoningen, J., Gauquelin, N., Babayigit, A., D'Haen, J., D'Olieslaeger, L., Ethirajan, A., Verbeeck, J., Manca, J., Mosconi, E., et al. (2015). Intrinsic Thermal Instability of Methylammonium Lead Trihalide Perovskite. *Advanced Energy Materials* *5*, 1500477. <https://doi.org/10.1002/aenm.201500477>.
13. Zhou, J., Xu, X., Wu, H., Wang, J., Lou, L., Yin, K., Gong, Y., Shi, J., Luo, Y., Li, D., et al. (2023). Control of the phase evolution of kesterite by tuning of the selenium partial

- pressure for solar cells with 13.8% certified efficiency. *Nature Energy* 8, 526-535. 10.1038/s41560-023-01251-6.
14. Wang, A., He, M., Green, M.A., Sun, K., and Hao, X. (2023). A Critical Review on the Progress of Kesterite Solar Cells: Current Strategies and Insights. *Advanced Energy Materials* 13, 2203046. <https://doi.org/10.1002/aenm.202203046>.
 15. Polman, A., Knight, M., Garnett, E.C., Ehrler, B., and Sinke, W.C. (2016). Photovoltaic materials: Present efficiencies and future challenges. *Science* 352, aad4424. doi:10.1126/science.aad4424.
 16. Zakutayev, A. (2017). Brief review of emerging photovoltaic absorbers. *Current Opinion in Green and Sustainable Chemistry* 4, 8-15. <https://doi.org/10.1016/j.cogsc.2017.01.002>.
 17. Zakutayev, A., Major, J.D., Hao, X., Walsh, A., Tang, J., Todorov, T.K., Wong, L.H., and Saucedo, E. (2021). Emerging inorganic solar cell efficiency tables (version 2). *Journal of Physics: Energy* 3, 032003. 10.1088/2515-7655/abebca.
 18. Choi, J.W., Shin, B., Gorai, P., Hoyer, R.L.Z., and Palgrave, R. (2022). Emerging Earth-Abundant Solar Absorbers. *ACS Energy Letters* 7, 1553-1557. 10.1021/acsenerylett.2c00516.
 19. Saparov, B. (2022). Next Generation Thin-Film Solar Absorbers Based on Chalcogenides. *Chemical Reviews* 122, 10575-10577. 10.1021/acs.chemrev.2c00346.
 20. Gershon, T., Lee, Y.S., Antunez, P., Mankad, R., Singh, S., Bishop, D., Gunawan, O., Hopstaken, M., and Haight, R. (2016). Photovoltaic Materials and Devices Based on the Alloyed Kesterite Absorber (Ag_xCu_{1-x})₂ZnSnSe₄. *Advanced Energy Materials* 6, 1502468. <https://doi.org/10.1002/aenm.201502468>.
 21. Qi, Y.-F., Kou, D.-X., Zhou, W.-H., Zhou, Z.-J., Tian, Q.-W., Meng, Y.-N., Liu, X.-S., Du, Z.-L., and Wu, S.-X. (2017). Engineering of interface band bending and defects elimination via a Ag-graded active layer for efficient (Cu,Ag)₂ZnSn(S,Se)₄ solar cells. *Energy & Environmental Science* 10, 2401-2410. 10.1039/C7EE01405H.
 22. Su, Z., Liang, G., Fan, P., Luo, J., Zheng, Z., Xie, Z., Wang, W., Chen, S., Hu, J., Wei, Y., et al. (2020). Device Postannealing Enabling over 12% Efficient Solution-Processed Cu₂ZnSnS₄ Solar Cells with Cd²⁺ Substitution. *Advanced Materials* 32, 2000121. <https://doi.org/10.1002/adma.202000121>.
 23. Giraldo, S., Jehl, Z., Placidi, M., Izquierdo-Roca, V., Pérez-Rodríguez, A., and Saucedo, E. (2019). Progress and Perspectives of Thin Film Kesterite Photovoltaic Technology: A Critical Review. *Advanced Materials* 31, 1806692. <https://doi.org/10.1002/adma.201806692>.
 24. Saliba, M., Matsui, T., Seo, J.-Y., Domanski, K., Correa-Baena, J.-P., Nazeeruddin, M.K., Zakeeruddin, S.M., Tress, W., Abate, A., Hagfeldt, A., and Grätzel, M. (2016). Cesium-containing triple cation perovskite solar cells: improved stability, reproducibility and high efficiency. *Energy & Environmental Science* 9, 1989-1997. 10.1039/C5EE03874J.
 25. Gratiá, P., Grancini, G., Audinot, J.-N., Jeanbourquin, X., Mosconi, E., Zimmermann, I., Dowsett, D., Lee, Y., Grätzel, M., De Angelis, F., et al. (2016). Intrinsic Halide Segregation at Nanometer Scale Determines the High Efficiency of Mixed Cation/Mixed Halide Perovskite Solar Cells. *Journal of the American Chemical Society* 138, 15821-15824. 10.1021/jacs.6b10049.

26. McMeekin, D.P., Sadoughi, G., Rehman, W., Eperon, G.E., Saliba, M., Hörantner, M.T., Haghighirad, A., Sakai, N., Korte, L., Rech, B., et al. (2016). A mixed-cation lead mixed-halide perovskite absorber for tandem solar cells. *Science* *351*, 151-155. doi:10.1126/science.aad5845.
27. Yu, L., and Zunger, A. (2012). Identification of Potential Photovoltaic Absorbers Based on First-Principles Spectroscopic Screening of Materials. *Physical Review Letters* *108*, 068701. 10.1103/PhysRevLett.108.068701.
28. Körbel, S., Marques, M.A.L., and Botti, S. (2016). Stability and electronic properties of new inorganic perovskites from high-throughput ab initio calculations. *Journal of Materials Chemistry C* *4*, 3157-3167. 10.1039/C5TC04172D.
29. Zhao, X.-G., Yang, J.-H., Fu, Y., Yang, D., Xu, Q., Yu, L., Wei, S.-H., and Zhang, L. (2017). Design of Lead-Free Inorganic Halide Perovskites for Solar Cells via Cation-Transmutation. *Journal of the American Chemical Society* *139*, 2630-2638. 10.1021/jacs.6b09645.
30. Chakraborty, S., Xie, W., Mathews, N., Sherburne, M., Ahuja, R., Asta, M., and Mhaisalkar, S.G. (2017). Rational Design: A High-Throughput Computational Screening and Experimental Validation Methodology for Lead-Free and Emergent Hybrid Perovskites. *ACS Energy Letters* *2*, 837-845. 10.1021/acsenergylett.7b00035.
31. Huo, Z., Wei, S.-H., and Yin, W.-J. (2018). High-throughput screening of chalcogenide single perovskites by first-principles calculations for photovoltaics. *Journal of Physics D: Applied Physics* *51*, 474003. 10.1088/1361-6463/aae1ee.
32. Fabini, D.H., Koerner, M., and Seshadri, R. (2019). Candidate Inorganic Photovoltaic Materials from Electronic Structure-Based Optical Absorption and Charge Transport Proxies. *Chemistry of Materials* *31*, 1561-1574. 10.1021/acs.chemmater.8b04542.
33. Kang, Y., Youn, Y., Han, S., Park, J., and Oh, C.-S. (2019). Computational Screening of Indirect-Gap Semiconductors for Potential Photovoltaic Absorbers. *Chemistry of Materials* *31*, 4072-4080. 10.1021/acs.chemmater.9b00708.
34. Cai, Y., Xie, W., Teng, Y.T., Harikesh, P.C., Ghosh, B., Huck, P., Persson, K.A., Mathews, N., Mhaisalkar, S.G., Sherburne, M., and Asta, M. (2019). High-throughput Computational Study of Halide Double Perovskite Inorganic Compounds. *Chemistry of Materials* *31*, 5392-5401. 10.1021/acs.chemmater.9b00116.
35. Li, Y., and Yang, K. (2019). High-throughput computational design of organic–inorganic hybrid halide semiconductors beyond perovskites for optoelectronics. *Energy & Environmental Science* *12*, 2233-2243. 10.1039/C9EE01371G.
36. Dahliah, D., Brunin, G., George, J., Ha, V.-A., Rignanese, G.-M., and Hautier, G. (2021). High-throughput computational search for high carrier lifetime, defect-tolerant solar absorbers. *Energy & Environmental Science* *14*, 5057-5073. 10.1039/D1EE00801C.
37. Mannodi-Kanakithodi, A., and Chan, M.K.Y. (2022). Data-driven design of novel halide perovskite alloys. *Energy & Environmental Science* *15*, 1930-1949. 10.1039/D1EE02971A.
38. Zakutayev, A., Caskey, C.M., Fioretti, A.N., Ginley, D.S., Vidal, J., Stevanovic, V., Tea, E., and Lany, S. (2014). Defect Tolerant Semiconductors for Solar Energy Conversion. *The Journal of Physical Chemistry Letters* *5*, 1117-1125. 10.1021/jz5001787.

39. Brandt, R.E., Stevanović, V., Ginley, D.S., and Buonassisi, T. (2015). Identifying defect-tolerant semiconductors with high minority-carrier lifetimes: beyond hybrid lead halide perovskites. *MRS Communications* 5, 265-275. 10.1557/mrc.2015.26.
40. Steirer, K.X., Schulz, P., Teeter, G., Stevanovic, V., Yang, M., Zhu, K., and Berry, J.J. (2016). Defect Tolerance in Methylammonium Lead Triiodide Perovskite. *ACS Energy Letters* 1, 360-366. 10.1021/acseenergylett.6b00196.
41. Walsh, A., and Zunger, A. (2017). Instilling defect tolerance in new compounds. *Nature Materials* 16, 964-967. 10.1038/nmat4973.
42. Brandt, R.E., Poindexter, J.R., Gorai, P., Kurchin, R.C., Hoye, R.L.Z., Nienhaus, L., Wilson, M.W.B., Polizzotti, J.A., Sereika, R., Žaltauskas, R., et al. (2017). Searching for “Defect-Tolerant” Photovoltaic Materials: Combined Theoretical and Experimental Screening. *Chemistry of Materials* 29, 4667-4674. 10.1021/acs.chemmater.6b05496.
43. Park, J.S., Kim, S., Xie, Z., and Walsh, A. (2018). Point defect engineering in thin-film solar cells. *Nature Reviews Materials* 3, 194-210. 10.1038/s41578-018-0026-7.
44. Kim, G.-W., and Petrozza, A. (2020). Defect Tolerance and Intolerance in Metal-Halide Perovskites. *Advanced Energy Materials* 10, 2001959. <https://doi.org/10.1002/aenm.202001959>.
45. Huang, Y.-T., Kavanagh, S.R., Scanlon, D.O., Walsh, A., and Hoye, R.L.Z. (2021). Perovskite-inspired materials for photovoltaics and beyond—from design to devices. *Nanotechnology* 32, 132004. 10.1088/1361-6528/abcf6d.
46. Jain, A., Ong, S.P., Hautier, G., Chen, W., Richards, W.D., Dacek, S., Cholia, S., Gunter, D., Skinner, D., Ceder, G., and Persson, K.A. (2013). Commentary: The Materials Project: A materials genome approach to accelerating materials innovation. *APL Materials* 1. 10.1063/1.4812323.
47. Bergerhoff, G., Hundt, R., Sievers, R., and Brown, I.D. (1983). The inorganic crystal structure data base. *Journal of Chemical Information and Computer Sciences* 23, 66-69. 10.1021/ci00038a003.
48. Heyd, J., Scuseria, G.E., and Ernzerhof, M. (2006). Erratum: “Hybrid functionals based on a screened Coulomb potential” [*J. Chem. Phys.* 118, 8207 (2003)]. *The Journal of Chemical Physics* 124. 10.1063/1.2204597.
49. Kirchartz, T., and Rau, U. (2018). What Makes a Good Solar Cell? *Advanced Energy Materials* 8, 1703385. <https://doi.org/10.1002/aenm.201703385>.
50. Kim, S., Márquez, J.A., Unold, T., and Walsh, A. (2020). Upper limit to the photovoltaic efficiency of imperfect crystals from first principles. *Energy & Environmental Science* 13, 1481-1491. 10.1039/D0EE00291G.
51. Sun, Y.-Y., Agiorgousis, M.L., Zhang, P., and Zhang, S. (2015). Chalcogenide Perovskites for Photovoltaics. *Nano Letters* 15, 581-585. 10.1021/nl504046x.
52. Wei, X., Hui, H., Zhao, C., Deng, C., Han, M., Yu, Z., Sheng, A., Roy, P., Chen, A., Lin, J., et al. (2020). Realization of BaZrS₃ chalcogenide perovskite thin films for optoelectronics. *Nano Energy* 68, 104317. <https://doi.org/10.1016/j.nanoen.2019.104317>.
53. Klüfers, P., Neumann, H., Mewis, A., and Schuster, H.-U. (1980). AB₂X₂-Verbindungen im CaAl₂Si₂-Typ, VIII [1] / AB₂X₂ Compounds with the CaAl₂Si₂ Structure, VIII [1]. *Zeitschrift für Naturforschung B* 35, 1317-1318. doi:10.1515/znb-1980-1029.

54. Klüfers, P., and Mewis, A. (1984). A B₂X₂- Verbindungen mit CaAl₂Si₂-Struktur. X. Zur Struktur neuer ternärer Erdalkaliphosphide und -arsenide *169*, 135-148. doi:10.1524/zkri.1984.169.14.135.
55. Liu, D., Peng, H., Huang, J., and Sa, R. (2022). Revealing the stability and optoelectronic properties of novel nitride and phosphide semiconductors: A DFT prediction. *Surfaces and Interfaces* *29*, 101740. <https://doi.org/10.1016/j.surfin.2022.101740>.
56. Savelsberg, G. (1978). Ternäre Pnictide und Chalkogenide von Alkalimetallen und IB- bzw. IIB-Elementen / On Ternary Pnictides and Chalkogenides of Alkaline Metals and IB-resp. II B-Elements. *Zeitschrift für Naturforschung B* *33*, 370-373. doi:10.1515/znb-1978-0404.
57. Antoniuk, E.R., Schindler, P., Schroeder, W.A., Dunham, B., Pianetta, P., Vecchione, T., and Reed, E.J. (2021). Novel Ultrabright and Air-Stable Photocathodes Discovered from Machine Learning and Density Functional Theory Driven Screening. *Advanced Materials* *33*, 2104081. <https://doi.org/10.1002/adma.202104081>.
58. DiSalvo, F.J., Trail, S.S., Yamane, H., and Brese, N.E. (1997). The crystal structure of Sr₆Cu₃N₅ with isolated, bent (Cu₂1N₃)⁷⁻ anions and the single crystal structural determination of SrCuN. *Journal of Alloys and Compounds* *255*, 122-129. [https://doi.org/10.1016/S0925-8388\(96\)02811-3](https://doi.org/10.1016/S0925-8388(96)02811-3).
59. Chern, M.Y., DiSalvo, F.J., Parise, J.B., and Goldstone, J.A. (1992). The structural distortion of the anti-perovskite nitride Ca₃AsN. *Journal of Solid State Chemistry* *96*, 426-435. [https://doi.org/10.1016/S0022-4596\(05\)80277-4](https://doi.org/10.1016/S0022-4596(05)80277-4).
60. Zheng, C., Hoffmann, R., Nesper, R., and Von Schnering, H.G. (1986). Site preferences and bond length differences in CaAl₂Si₂-type Zintl compounds. *Journal of the American Chemical Society* *108*, 1876-1884. 10.1021/ja00268a027.
61. Condrón, C.L., Kauzlarich, S.M., Gascoin, F., and Snyder, G.J. (2006). Thermoelectric properties and microstructure of Mg₃Sb₂. *Journal of Solid State Chemistry* *179*, 2252-2257. <https://doi.org/10.1016/j.jssc.2006.01.034>.
62. Zhang, J., Song, L., Pedersen, S.H., Yin, H., Hung, L.T., and Iversen, B.B. (2017). Discovery of high-performance low-cost n-type Mg₃Sb₂-based thermoelectric materials with multi-valley conduction bands. *Nature Communications* *8*, 13901. 10.1038/ncomms13901.
63. Peng, W., Petretto, G., Rignanese, G.-M., Hautier, G., and Zevalkink, A. (2018). An Unlikely Route to Low Lattice Thermal Conductivity: Small Atoms in a Simple Layered Structure. *Joule* *2*, 1879-1893. 10.1016/j.joule.2018.06.014.
64. May, A.F., McGuire, M.A., Singh, D.J., Ma, J., Delaire, O., Huq, A., Cai, W., and Wang, H. (2012). Thermoelectric transport properties of CaMg₂Bi₂, EuMg₂Bi₂, and YbMg₂Bi₂. *Physical Review B* *85*, 035202. 10.1103/PhysRevB.85.035202.
65. Sun, J., and Singh, D.J. (2017). Thermoelectric properties of AMg₂X₂, AZn₂Sb₂ (A = Ca, Sr, Ba; X = Sb, Bi), and Ba₂ZnX₂ (X = Sb, Bi) Zintl compounds. *Journal of Materials Chemistry A* *5*, 8499-8509. 10.1039/C6TA11234J.
66. Wang, T., Daiber, B., Frost, J.M., Mann, S.A., Garnett, E.C., Walsh, A., and Ehrler, B. (2017). Indirect to direct bandgap transition in methylammonium lead halide perovskite. *Energy & Environmental Science* *10*, 509-515. 10.1039/C6EE03474H.

67. Kumagai, Y., Kavanagh, S.R., Suzuki, I., Omata, T., Walsh, A., Scanlon, D.O., and Morito, H. (2023). Alkali Mono-Pnictides: A New Class of Photovoltaic Materials by Element Mutation. *PRX Energy* 2, 043002. 10.1103/PRXEnergy.2.043002.
68. Ricci, F., Chen, W., Aydemir, U., Snyder, G.J., Rignanese, G.-M., Jain, A., and Hautier, G. (2017). An ab initio electronic transport database for inorganic materials. *Scientific Data* 4, 170085. 10.1038/sdata.2017.85.
69. Vukmirović, N. (2021). Calculations of electron mobility in II-VI semiconductors. *Physical Review B* 104, 085203. 10.1103/PhysRevB.104.085203.
70. Ganose, A.M., Park, J., Faghaninia, A., Woods-Robinson, R., Persson, K.A., and Jain, A. (2021). Efficient calculation of carrier scattering rates from first principles. *Nature Communications* 12, 2222. 10.1038/s41467-021-22440-5.
71. Monserrat, B., Park, J.-S., Kim, S., and Walsh, A. (2018). Role of electron-phonon coupling and thermal expansion on band gaps, carrier mobility, and interfacial offsets in kesterite thin-film solar cells. *Applied Physics Letters* 112. 10.1063/1.5028186.
72. Poncé, S., Li, W., Reichardt, S., and Giustino, F. (2020). First-principles calculations of charge carrier mobility and conductivity in bulk semiconductors and two-dimensional materials. *Reports on Progress in Physics* 83, 036501. 10.1088/1361-6633/ab6a43.
73. Yin, W.-J., Yang, J.-H., Kang, J., Yan, Y., and Wei, S.-H. (2015). Halide perovskite materials for solar cells: a theoretical review. *Journal of Materials Chemistry A* 3, 8926-8942. 10.1039/C4TA05033A.
74. Yin, W.-J., Shi, T., and Yan, Y. (2014). Unusual defect physics in CH₃NH₃PbI₃ perovskite solar cell absorber. *Applied Physics Letters* 104. 10.1063/1.4864778.
75. Buin, A., Comin, R., Xu, J., Ip, A.H., and Sargent, E.H. (2015). Halide-Dependent Electronic Structure of Organolead Perovskite Materials. *Chemistry of Materials* 27, 4405-4412. 10.1021/acs.chemmater.5b01909.
76. Meggiolaro, D., Motti, S.G., Mosconi, E., Barker, A.J., Ball, J., Andrea Riccardo Perini, C., Deschler, F., Petrozza, A., and De Angelis, F. (2018). Iodine chemistry determines the defect tolerance of lead-halide perovskites. *Energy & Environmental Science* 11, 702-713. 10.1039/C8EE00124C.
77. Keeble, D.J., Wiktor, J., Pathak, S.K., Phillips, L.J., Dickmann, M., Durose, K., Snaith, H.J., and Egger, W. (2021). Identification of lead vacancy defects in lead halide perovskites. *Nature Communications* 12, 5566. 10.1038/s41467-021-25937-1.
78. Lyons, J.L., and Swift, M.W. (2023). Trends for Acceptor Dopants in Lead Halide Perovskites. *The Journal of Physical Chemistry C* 127, 12735-12740. 10.1021/acs.jpcc.3c01972.
79. Zhang, S.B., Wei, S.-H., Zunger, A., and Katayama-Yoshida, H. (1998). Defect physics of the CuInSe₂ chalcopyrite semiconductor. *Physical Review B* 57, 9642-9656. 10.1103/PhysRevB.57.9642.
80. Liu, J., Song, Y., Xu, X., Li, W., Yang, J., and Li, X. (2023). Identification of intrinsic defects and hydrogen passivation in InP using hybrid functional. *Journal of Applied Physics* 134. 10.1063/5.0164899.
81. Yuan, Z., Xiong, Y., and Hautier, G. (2023). First-principles study of intrinsic and hydrogen point defects in the earth-abundant photovoltaic absorber Zn₃P₂. *Journal of Materials Chemistry A*. 10.1039/D3TA03697A.

82. Zhang, S.B., Wei, S.-H., and Zunger, A. (1998). A phenomenological model for systematization and prediction of doping limits in II–VI and I–III–VI₂ compounds. *Journal of Applied Physics* *83*, 3192-3196. 10.1063/1.367120.
83. Savory, C.N., Ganose, A.M., Travis, W., Atri, R.S., Palgrave, R.G., and Scanlon, D.O. (2016). An assessment of silver copper sulfides for photovoltaic applications: theoretical and experimental insights. *Journal of Materials Chemistry A* *4*, 12648-12657. 10.1039/C6TA03376H.
84. Alkauskas, A., Yan, Q., and Van de Walle, C.G. (2014). First-principles theory of nonradiative carrier capture via multiphonon emission. *Physical Review B* *90*, 075202. 10.1103/PhysRevB.90.075202.
85. Li, J., Zhu, H.-F., Zhang, Y.-Y., Yuan, Z.-K., Chen, S., and Gong, X.-G. (2017). Large carrier-capture rate of Pbl antisite in CH₃NH₃PbI₃ induced by heavy atoms and soft phonon modes. *Physical Review B* *96*, 104103. 10.1103/PhysRevB.96.104103.
86. Zhang, X., Turiansky, M.E., Shen, J.-X., and Van de Walle, C.G. (2022). Defect tolerance in halide perovskites: A first-principles perspective. *Journal of Applied Physics* *131*. 10.1063/5.0083686.
87. Bagraev, N.T., and Mashkov, V.A. (1988). A mechanism for two-electron capture at deep level defects in semiconductors. *Solid State Communications* *65*, 1111-1117. [https://doi.org/10.1016/0038-1098\(88\)90904-0](https://doi.org/10.1016/0038-1098(88)90904-0).
88. Zhang, X., Turiansky, M.E., Shen, J.-X., and Van de Walle, C.G. (2020). Iodine interstitials as a cause of nonradiative recombination in hybrid perovskites. *Physical Review B* *101*, 140101. 10.1103/PhysRevB.101.140101.
89. Yang, J.-H., Yin, W.-J., Park, J.-S., Ma, J., and Wei, S.-H. (2016). Review on first-principles study of defect properties of CdTe as a solar cell absorber. *Semiconductor Science and Technology* *31*, 083002. 10.1088/0268-1242/31/8/083002.
90. Kavanagh, S.R., Walsh, A., and Scanlon, D.O. (2021). Rapid Recombination by Cadmium Vacancies in CdTe. *ACS Energy Letters* *6*, 1392-1398. 10.1021/acsenerylett.1c00380.
91. Dou, B., Falletta, S., Neugebauer, J., Freysoldt, C., Zhang, X., and Wei, S.-H. (2023). Chemical Trend of Nonradiative Recombination in Cu(In,Ga)Se₂ Alloys. *Physical Review Applied* *19*, 054054. 10.1103/PhysRevApplied.19.054054.
92. Li, J., Yuan, Z.-K., Chen, S., Gong, X.-G., and Wei, S.-H. (2019). Effective and Noneffective Recombination Center Defects in Cu₂ZnSnS₄: Significant Difference in Carrier Capture Cross Sections. *Chemistry of Materials* *31*, 826-833. 10.1021/acs.chemmater.8b03933.
93. Kim, S., Park, J.-S., Hood, Samantha N., and Walsh, A. (2019). Lone-pair effect on carrier capture in Cu₂ZnSnS₄ solar cells. *Journal of Materials Chemistry A* *7*, 2686-2693. 10.1039/C8TA10130B.
94. Singh, P., and Ravindra, N.M. (2012). Temperature dependence of solar cell performance—an analysis. *Solar Energy Materials and Solar Cells* *101*, 36-45. <https://doi.org/10.1016/j.solmat.2012.02.019>.
95. Reid, O.G., Moore, D.T., Li, Z., Zhao, D., Yan, Y., Zhu, K., and Rumbles, G. (2017). Quantitative analysis of time-resolved microwave conductivity data. *Journal of Physics D: Applied Physics* *50*, 493002. 10.1088/1361-6463/aa9559.
96. Savenije, T.J., Ferguson, A.J., Kopidakis, N., and Rumbles, G. (2013). Revealing the Dynamics of Charge Carriers in Polymer:Fullerene Blends Using Photoinduced Time-

- Resolved Microwave Conductivity. *The Journal of Physical Chemistry C* **117**, 24085-24103. 10.1021/jp406706u.
97. Blackburn, J.L., Zhang, H., Myers, A.R., Dunklin, J.R., Coffey, D.C., Hirsch, R.N., Vigil-Fowler, D., Yun, S.J., Cho, B.W., Lee, Y.H., et al. (2020). Measuring Photoexcited Free Charge Carriers in Mono- to Few-Layer Transition-Metal Dichalcogenides with Steady-State Microwave Conductivity. *The Journal of Physical Chemistry Letters* **11**, 99-107. 10.1021/acs.jpcllett.9b03117.
 98. Scarpulla, M.A., McCandless, B., Phillips, A.B., Yan, Y., Heben, M.J., Wolden, C., Xiong, G., Metzger, W.K., Mao, D., Krasikov, D., et al. (2023). CdTe-based thin film photovoltaics: Recent advances, current challenges and future prospects. *Solar Energy Materials and Solar Cells* **255**, 112289. <https://doi.org/10.1016/j.solmat.2023.112289>.
 99. Hempel, H., Dennler, G., Müller, S., Larramona, G., Eichberger, R., and Unold, T. (2016). Charge carrier dynamics in Cu₂ZnSn(S/Se)₄ thin film solar cells measured by time resolved terahertz and microwave spectroscopy. 25-30 Sept. 2016. pp. 1-2.
 100. Xing, G., Mathews, N., Sun, S., Lim, S.S., Lam, Y.M., Grätzel, M., Mhaisalkar, S., and Sum, T.C. (2013). Long-Range Balanced Electron- and Hole-Transport Lengths in Organic-Inorganic CH₃NH₃PbI₃. *Science* **342**, 344-347. doi:10.1126/science.1243167.
 101. Stranks, S.D., Eperon, G.E., Grancini, G., Menelaou, C., Alcocer, M.J.P., Leijtens, T., Herz, L.M., Petrozza, A., and Snaith, H.J. (2013). Electron-Hole Diffusion Lengths Exceeding 1 Micrometer in an Organometal Trihalide Perovskite Absorber. *Science* **342**, 341-344. doi:10.1126/science.1243982.
 102. Jaramillo, R., Sher, M.-J., Ofori-Okai, B.K., Steinmann, V., Yang, C., Hartman, K., Nelson, K.A., Lindenberg, A.M., Gordon, R.G., and Buonassisi, T. (2016). Transient terahertz photoconductivity measurements of minority-carrier lifetime in tin sulfide thin films: Advanced metrology for an early stage photovoltaic material. *Journal of Applied Physics* **119**. 10.1063/1.4940157.
 103. Savenije, T.J., Guo, D., Caselli, V.M., and Hutter, E.M. (2020). Quantifying Charge-Carrier Mobilities and Recombination Rates in Metal Halide Perovskites from Time-Resolved Microwave Photoconductivity Measurements. *Advanced Energy Materials* **10**, 1903788. <https://doi.org/10.1002/aenm.201903788>.
 104. Hempel, H., Savenije, T.J., Stolterfoht, M., Neu, J., Failla, M., Paingad, V.C., Kužel, P., Heilweil, E.J., Spies, J.A., Schleuning, M., et al. (2022). Predicting Solar Cell Performance from Terahertz and Microwave Spectroscopy. *Advanced Energy Materials* **12**, 2102776. <https://doi.org/10.1002/aenm.202102776>.
 105. Ferguson, A.J., Kopidakis, N., Shaheen, S.E., and Rumbles, G. (2008). Quenching of Excitons by Holes in Poly(3-hexylthiophene) Films. *The Journal of Physical Chemistry C* **112**, 9865-9871. 10.1021/jp7113412.
 106. Kroeze, J.E., Savenije, T.J., and Warman, J.M. (2004). Electrodeless Determination of the Trap Density, Decay Kinetics, and Charge Separation Efficiency of Dye-Sensitized Nanocrystalline TiO₂. *Journal of the American Chemical Society* **126**, 7608-7618. 10.1021/ja039303u.
 107. Herz, L.M. (2017). Charge-Carrier Mobilities in Metal Halide Perovskites: Fundamental Mechanisms and Limits. *ACS Energy Letters* **2**, 1539-1548. 10.1021/acsenerylett.7b00276.

